

The Experimental and Numerical Analysis of the Joining Processes for Air Conditioning Systems

M.St. Węglowski, D. Miara, S. Błacha, J. Dworak, J. Rykała, K. Kwieciński, J. Pikula, G. Ziobro, A. Szafron, P. Zimierska-Nowak, M. Richert, P. Noga

I. INTRODUCTION

Abstract—In the paper the results of welding of car's air-conditioning elements are presented. These systems based on, mainly, the environmental unfriendly refrigerants. Thus, the producers of cars will have to stop using traditional refrigerant and to change it to carbon dioxide (R744). This refrigerant is environmental friendly. However, it should be noted that the air condition system working with R744 refrigerant operates at high temperature (up to 150 °C) and high pressure (up to 130 bar). These two parameters are much higher than for other refrigerants. Thus new materials, design as well as joining technologies are strongly needed for these systems. AISI 304 and 316L steels as well as aluminium alloys 5xxx are ranked among the prospective materials. As a joining process laser welding, plasma welding, electron beam welding as well as high rotary friction welding can be applied. In the study, the metallographic examination based on light microscopy as well as SEM was applied to estimate the quality of welded joints. The analysis of welding was supported by numerical modelling based on Sysweld software. The results indicated that using laser, plasma and electron beam welding, it is possible to obtain proper quality of welds in stainless steel. Moreover, high rotary friction welding allows to guarantee the metallic continuity in the aluminium welded area. The metallographic examination revealed that the grain growth in the heat affected zone (HAZ) in laser and electron beam welded joints were not observed. It is due to low heat input and short welding time. The grain growth and subgrains can be observed at room temperature when the solidification mode is austenitic. This caused low microstructural changes during solidification. The columnar grain structure was found in the weld metal. Meanwhile, the equiaxed grains were detected in the interface. The numerical modelling of laser welding process allowed to estimate the temperature profile in the welded joint as well as predicts the dimensions of welds. The agreement between FEM analysis and experimental data was achieved.

Keywords—Car's air-conditioning, microstructure, numerical modelling, welding.

M.St. Węglowski is with the Institute of Welding, Gliwice 44-100, Poland (phone: +48 32 3358236; fax: +48 32 2314652; e-mail: marek.weglowski@is.gliwice.pl).

D. Miara, S. Błacha, J. Dworak, J. Rykała, K. Kwieciński, and J. Pikula is with the Institute of Welding, Gliwice 44-100, Poland (e-mail: damian.miara@is.gliwice.pl, sylwester.blacha@is.gliwice.pl, jerzy.dworak@is.gliwice.pl, janusz.rykala@is.gliwice.pl, krzysztof.kwiecinski@is.gliwice.pl, janusz.pikula@is.gliwice.pl).

G. Ziobro, A. Szafron, and P. Zimierska-Nowak are with Maflow Member of Boryszew Group, Tychy 43-100, Poland (e-mail: grzegorz.ziobro@maflow.com, adam.szafron@maflow.com, patrycja.zimierska@maflow.com).

M. Richert and P. Noga is with AGH University of Science and Technology, Kraków 30-059, Poland (e-mail: mrichert@agh.edu.pl, pionoga@agh.edu.pl).

CAR air conditioning has become more and more popular. Nowadays, it is difficult to buy a new car without air cooling system. A thermal comfort for passengers by using the air conditioning system is ensured. Moreover, the defogging of windows is improved and thus an increase in safety can be observed. It should be noted that the automobile air conditioning system is different from the air conditioning facilities in buildings. The working conditions in an automobile vary markedly if compared to buildings both in time and space [1].

When a car is driven or parked in the sun, heat enters the vehicle from many sources (Fig. 1). All of these and other miscellaneous heat sources increase the air temperature within the vehicle. In a high ambient temperature situation, (e.g. on a 37 °C day), the interior of a vehicle left standing in the sun with windows closed could reach 65-70 °C [2].

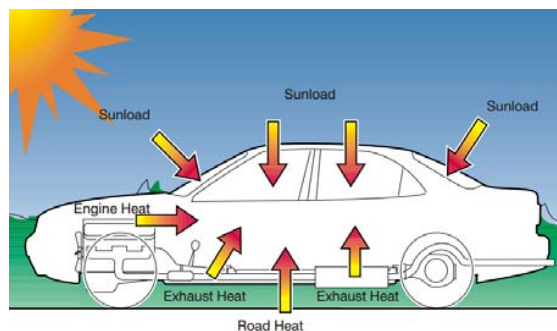


Fig. 1 Factors causing the increase of the temperature in a car [2]

The refrigerant commonly used in car air conditioning (CAC) systems is tetrafluoroethane, R134a for short. R134a demonstrates a high global potential (GWP), which is 1,300 times higher or, considering recent data of the Intergovernmental Panel on Climate Change (IPCC) [3], even 1430 times higher – than that of CO₂. A comparison of most popular refrigerants is given in Table I. A car equipped with air conditioning produces additional emissions corresponding to 7 grams of CO₂ per driven kilometer by the continuous release of R134a from the system. Thus, car air conditioning systems are the single most important source of fluorinated greenhouse gases, mainly due to high emissions during their operation and their large numbers. More than 400 million vehicles worldwide are equipped with CACs.

TABLE I
COMPARISON OF REFRIGERANTS [2]-[5]

| Commercial name | R12 | R134a | R1234yf | R744 |
|--------------------------|-------|-------|---------|-------|
| Ozone depleting | 1.0 | 0.03 | 0 | 0 |
| Global warming potential | 10600 | 1430 | 4 | 1 |
| Boiling point | -29.6 | -26.3 | -29.0 | -78.4 |

The climate experts of the IPCC expect that there were nearly 1 billion air-conditioned vehicles by 2015. In 2015 alone, refrigerant release to the atmosphere amounted to at least 270 million tonnes of CO₂ equivalent, contributing to climate change. In Germany, almost 2300 tonnes of the fluorinated refrigerant R134a were emitted to the atmosphere in 2006 alone. This is equivalent to almost 3 million tonnes of CO₂, which is as much carbon dioxide as is emitted via the exhaust gas pipe of 1.7 million small-sized vehicles each driving 15000 kilometres per year [2]-[5].

The European directives 2006/40/EC [4] on the greenhouse gasses elimination demand to stop using traditional refrigerant and to change it to R744 medium in air conditioning installation. The R744 (CO₂) refrigerant is environmentally friendly medium if compared with standard solution such as R12, R134a or R1234yf and safer for passengers than R1234yf.

R744 characterised by the non-standard thermodynamic parameters leading to high pressure and temperature, needed special materials to design the shape and develop the technology of production of specific elements of conduits. It is also required the developing of the technologies joining the whole structure and meeting the requirements for exploitation of the new product.

To produce the welded joints of stainless steels, many different joining technologies can be applied [6]: laser welding [7], plasma welding [8], electron beam welding [9] as well as high rotary friction welding [10]. However, it should be noted that the welding metallurgy of these steels is complicated. Austenitic stainless steels are faced with the main three types of risks [11]: embrittlement by phase V for the most alloyed steels, occurring during the usage but is very limited while welding operations as the heating and cooling speeds are in general too fast to start the precipitation; hot cracking, which is a real risk during welding; the precipitation of chromium carbides (Cr₂₃C₆) which is tantamount to the risk of intergranular corrosion [12], [13].

This paper describes the influence of the selected welding process on the macrostructure and microstructure of welded joints of AISI 304, AISI 316L steels and aluminium alloy grade AA5049. The results of numerical modelling of laser welding of stainless steels were also presented.

II. EXPERIMENTAL DETAILS

To produce the test welded joints of stainless steels, three different joining technologies were applied: laser welding, electron beam welding and plasma welding. Additionally, for aluminium parts, a high speed friction welding was adopted. Figs. 2 and 3 show the components made of steel and

aluminium respectively.



Fig. 2 The steel's components nipple and corrugated hose

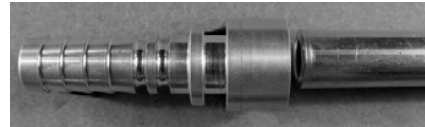


Fig. 3 The aluminium's components nipple and tube

AISI 406 (nipple) and AISI 316L (corrugated hose) steels were chosen for the present study. Their chemical compositions are shown in Table II.

TABLE II
CHEMICAL COMPOSITION OF AISI 304 AND AISI 316L STEELS

| Steel | Elements wt. [%] | | | | | | |
|----------|------------------|-----|-----------|-----------|-------|------|-----|
| | C | Mn | Cr | Ni | P | S | Si |
| AISI304 | 0.08 | 2.0 | 18.0-20.0 | 8.0-10.5 | 0.045 | 0.03 | 1.0 |
| AISI316L | 0.03 | 2.0 | 16.0-18.0 | 10.0-14.0 | 0.045 | 0.03 | 1.0 |

The welded joints, in a butt configuration, were fabricated using an pulsed laser TruPulse 103 (Fig. 4), plasma welding machine model MSP-51, electron beam welding machine model XW150:30/756 and Harm&Wende high-speed friction welding machine RSM 400. All specimens were welded at Instytut Spawalnictwa (Institute of Welding) in Gliwice.

Microstructure was observed by an Eclipse MA 200 (Nikon) light microscope (LM) as well as scanning electron microscope (SEM) Hitachi SU 70. The samples to microscopy observations were polished mechanically with the application of Struers equipment and technique.

The numerical modelling of laser welding was performed using the SYSWELD software. The heat source was described in the form of a truncated cone, whereas the amount of energy was determined on the basis of a real Nd:YAG laser welding process. The verification of numerical modelling based on temperature measurements were carried out. The thermocouples type K was applied.

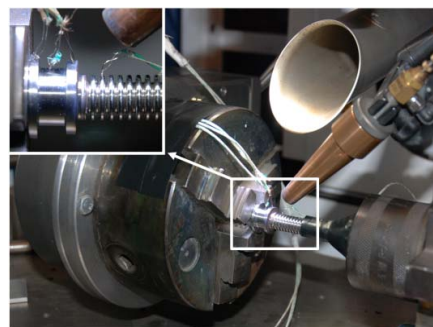


Fig. 4 Laser welding setup

III. RESULTS AND DISCUSSION

The microstructures of the investigated AISI 304 and AISI 316L steels in their as-delivered state are presented in Figs. 5 and 6, respectively. Steels displayed an austenitic structure with a twin.

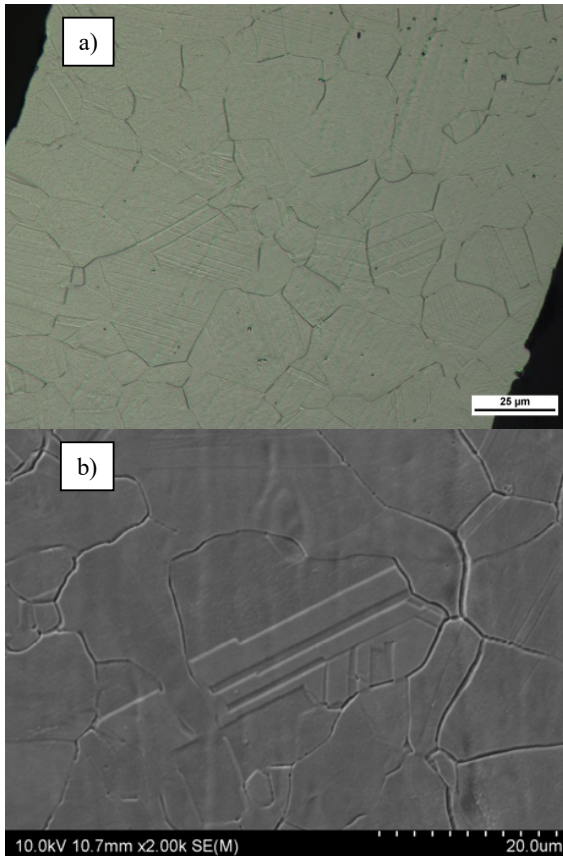


Fig. 5 The microstructure of AISI 304 base metal used in the study, (a) light microscope, (b) SEM

The welding parameters are as follows: impuls shape – CrNi, max power 1 kW, beam diameter 0.8, 0.6 and 0.4 mm (Fig. 7), rotational speed 4 RPM. Argon as a shielding gas was used. It can be seen that the fusion zones depend on welding parameters. Decrease in the beam diameter caused an increase in the penetration depth and a decrease in the width of the welds (decrease in the beam diameter, at the constant power, caused an increase in a power density). Moreover, the welding trails have shown that the preparation methods of elements for welding are important. Due to the small thickness of the corrugated hoses, stability of welding process is highly dependent on the exact adherence of elements welded to each other.

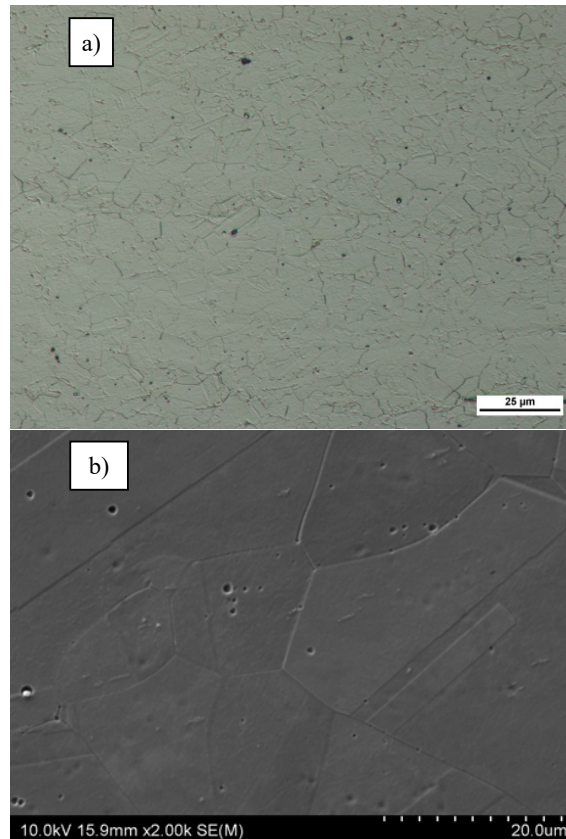


Fig. 6 The microstructure of AISI 316L base metal used in the study, (a) light microscope, (b) SEM

The appearance of small misalignment can cause local lack of welds to slightly melt the edge of the materials to be joined without the metallic continuity. In Fig. 7, it is clearly shown that the impulse laser technique was adopted for welding, 5 “separated” welds can be distinguished. Due to low heat input and welding time, grain growth in the HAZ was not observed. If the solidification mode is austenitic, the grain growth and subgrains can be observed at room temperature due to low microstructural changes during solidification. The grain structure in the weld metal was found to be columnar which was gradually transitioned to equiaxed grain in the interface [12], [13] (see Fig. 8). The fusion zone contains a mixture of fully austenitic and ferrite-austenitic structures. Laser welding weld metal microstructures consisting of δ -Ferrite as the primary solidification phase. It should be noted, that a high density chromium in the core of the δ -ferrite dendrites can be observed. While in the outer portions, lower chromium contents are observed. This is caused by the fact that the core forms at the beginning of solidification process and outer regions form as temperature decreases. Moreover, the outer portions of the dendrites having less chromium content transform to austenite and chromium rich skeleton of δ -ferrite at the dendrite cores can be created. This skeletal ferrite is called lacy or lathy ferrite [11]. Similar situation for electron beam (EB) welded joint can be observed. The macrostructure of EB welded joints in Fig. 9 was presented.

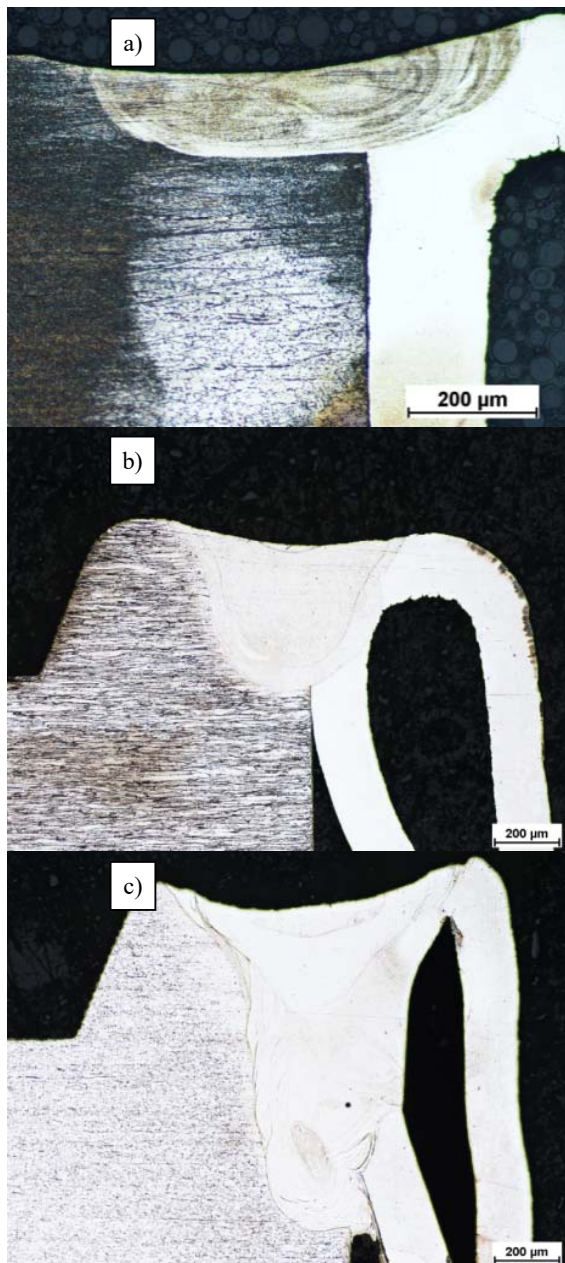


Fig. 7 The macrostructure of the laser beam welded joints at different beam diameters: (a) 0.8 mm, (b) 0.6 mm, (c) 0.4 mm

The EB welding process at the following parameters was carried out: accelerated voltage $U=150$ kV, focus=725 mA, beam current $I=0.8$ mA, $v=1500$ mm/min (300 RPM). The continuous EB was used during welding. The EB welding process in vacuum environment was carried out ($P=5 \cdot 10^{-5}$ mbar). As we can see, the good quality of EB welded joint can be achieved. The main difference is in a shape of fusion zone. For laser beam, the width of weld is 0.7 mm and for EB weld is 0.75 mm. However, the volume of weld for EB process is higher than for laser welding.

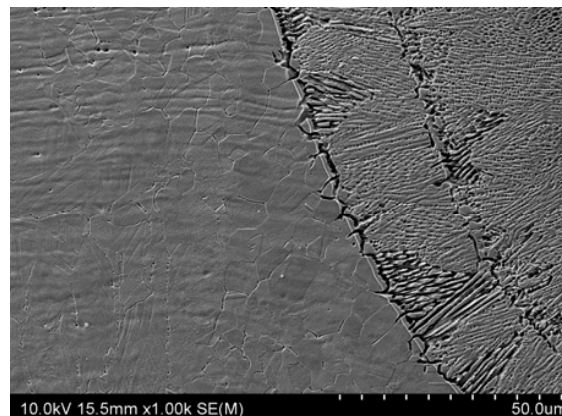


Fig. 8 Microstructure of laser welded joint



Fig. 9 The macrostructure of the EB welded joint

For the plasma arc welded joint the different situation can be observed. The macrostructure of a welded joint is shown in Fig. 10. The welded joint was manufactured at the following welding parameters: welding current $I=8.5$ A, arc voltage=22.5 V, welding speed $\omega=3$ RPM, 100%Ar as a plasma gas and 97%Ar+3% H_2 as shielding gas. It should be noticed that longer cooling time $t_{8/5}$ caused wider HAZ. Therefore, despite the partial solid-state phase transformation on cooling, the HAZ is, in general, characterized by a coarse grain size. On the other hand, narrow (up to few μm) dark-sensitized zone along the fusion line has been formed probably due to the precipitation of grain boundary carbides. The region adjacent to the fusion line of the fusion zone is subjected to the initiation of primary ferrite solidification and dendritic growth from the liquid metal during cooling. Therefore, prior to complete solidification, interdendritic liquid became enriched with alloying elements (mostly carbon, nitrogen, nickel, and chromium) due to high alloy segregation (rejection of C, N, and Ni from δ -phase to surrounding liquid). Because of the higher concentration of austenitic stabilizing elements,

remaining liquid solidified in γ -phase and δ/δ interfaces became the potential site for carbide and nitride precipitations (mostly $M_{23}C_6$ and MX type) [13].

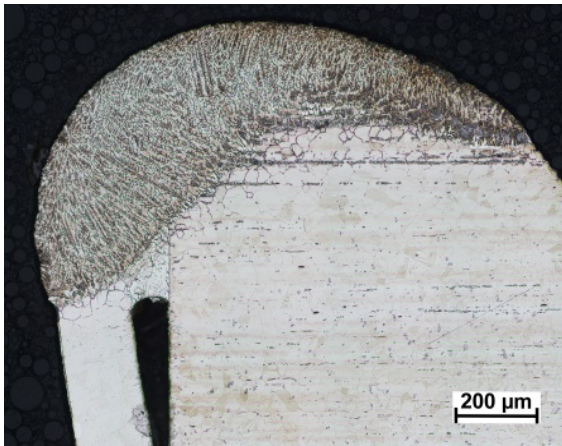


Fig. 10 The macrostructure of the plasma welded joint

The preliminary investigation of high speed friction welded joints has revealed that at the standard shapes of the nipple and tube (Fig. 3), it is not possible to achieve the proper quality of welded joint. The macrostructure of welded joint is shown in Fig. 11. As can be seen a tube undergoes intensive plastic deformation. The next investigation will be carried out. The main task will be to modify the shape of the nipple as well as a development of the welding process with plain pin. The welding process at the following parameters was carried out: rotation speed $\omega=20000$ RPM, friction time $t_f=0.8$ s, pressure force $F_p=1.0$ MPa, upsetting force $F_u=6.0$ MPa.

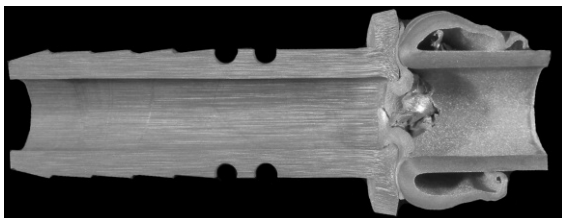


Fig. 11 The macrostructure of the friction welded joint

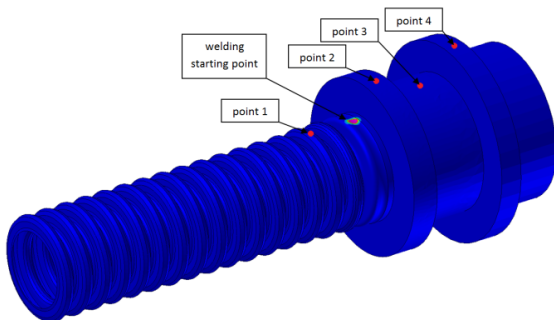


Fig. 12 Selected points of temperature measurements

For implementation, from the practical point of view, the

laser welding process should be the most interesting. Thus, numerical analysis of thermal phenomena occurring during laser beam welding as well as geometry of the welded joint was also carried out. The FEM model was validated based on the dimensions of a molten zone and temperature measurements in selected points of the welded components (Fig. 12).

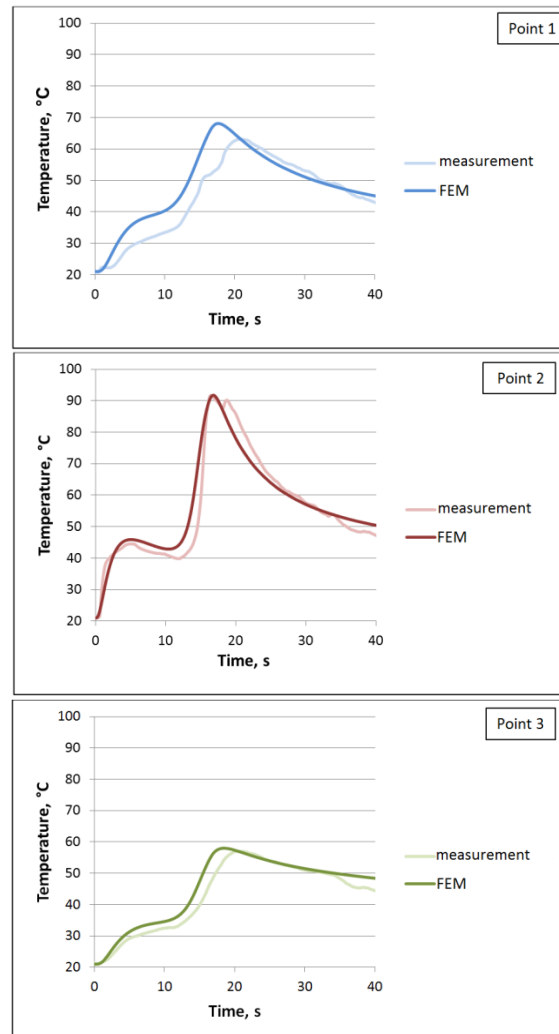


Fig. 13 Comparison of results of numerical modelling and experimental measurement of temperature at the selected points

Firstly, the temperature in the selected point was calculated. The results of numerical and experimental data were compared (Fig. 13). The highest difference between maximum temperature measured and that calculated using FEM was 7.9%, while medium difference of all measuring points was 3.9%. Small dimensions of components being welded (annularly corrugated hose wall thickness 0.2 mm and diameter 9.76 mm) and thereby possible imperfections in model geometry have significant impact on the calculation results. In addition, laser welding process is complex phenomenon, heat flow to the environment because of

shielding gas flow is nonlinear, so it can be stated that there is a good agreement of the results of temperature calculations to real results. In contrast to FEM of continuous laser welding or high frequency pulse laser welding, in case of low frequency pulse as in presented Nd:YAG welding process, it is necessary to treat every impulse as individual weld. Simulating low frequency pulse laser welding process as the continuous laser welding using the same laser power lead to the several times higher heat input. It could make possible to obtain proper dimensions of the molten zone, but calculated temperature field of welded components would be incorrect. Average power of Nd:YAG welding taken into consideration makes it possible to introduce correct heat amount in the aspect of total welding time (16.5 s), while power density in the time unit will be insufficient to obtain correct geometry of molten zone.

Secondly, the prediction of shape and dimension of the laser welded joint was carried out. Molten zone shape and dimensions were determined based on the 316L steel grade melting temperature range (1375 °C to 1400 °C) [14]. The FEM model of shape of welded joint has been compared to result of metallographic examination (Fig. 14). The good agreement of weld dimensions was confirmed. It should be noted that the laser welding process in impulse mode was carried out. On each cross section of laser welded joint, the multi welds can be observed (Figs. 7 and 14)

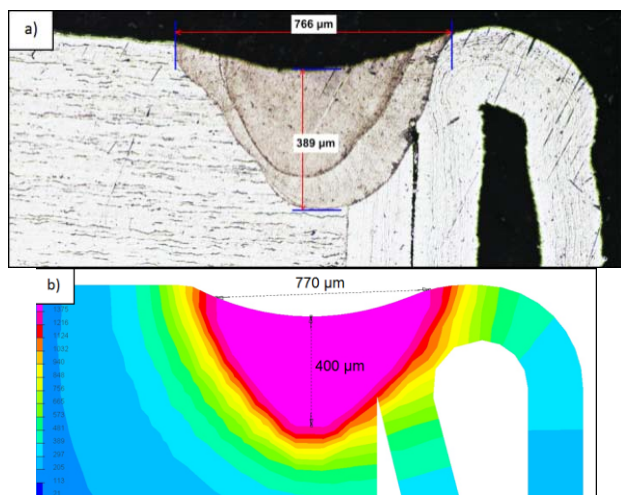


Fig. 14 Comparison of shape and dimensions of laser welded joint, (a) experimental measurement based on metallographic examination, (b) numerical modelling

IV. CONCLUSION

This paper describes the influence of the selected welding process on the macrostructure and microstructure of welded joints of AISI 304 and AISI 316L steels as well as AA5049 aluminium alloy. The results of this research are summarized as:

- the welding process has dominant influence on geometry and macrostructure of welded joints,
- the proper quality of steel welded joints for laser welding, EB welding as well as plasma arc welding can be

achieved,

- the high speed friction welding guarantees the proper quality of aluminium welded joint, however the technology should be developed,
- the numerical models allow to predict of temperature as well as dimension of the welded joint for laser welding.

ACKNOWLEDGMENT

This work has been performed with funding from National Centre for Research and Development in Poland within the frame of the research grant No PBS3/B5/43/2015 entitled: "The choice of materials and the development of the construction elements of air conditioning elements designed to work with the new refrigerant R744".

REFERENCES

- [1] Janotkova, M. Pavelek, New Trends in the Field of Automobile Air Conditioning. <https://www.aiha.org/aihce06/handouts/janotkova.pdf> (Created 2006.05.03).
- [2] Arizone, Automotive Air Conditioning Training Manual <http://www.ariazone.com.mk/pdf/Automotive%20Air%20Conditioning%20Training%20Manual.pdf> (Created 2007.06.02).
- [3] Natural refrigerants – CO₂-based air conditioning system put to practical testing. <http://www.umweltbundesamt.de/sites/default/files/medien/publikation/long/3654.pdf> (Created 2009.06.08).
- [4] Directive 2006/40/EC of the European Parliament and of the Council of 17 May 2006 relating to emissions from air-conditioning systems in motor vehicles and amending Council Directive 70/156/EEC
- [5] M. Mohanraj, S. Jayaraj, C. Muraleedharan, "Environment friendly alternatives to halogenated refrigerants—A review". International Journal of Greenhouse Gasses Control, vol. 3, pp. 108-119, 2009.
- [6] K.S. Prasad, Ch. Rao, D.N. Rao, "A review on welding of AISI 304L austenitic stainless steel", J. Manuf. Sci. Prod., vol. 14, pp. 1-11, 2014.
- [7] M.St. Węglowski, S. Stano, G. Michta, et al., "Structural characterization of Nd:YAG laser welded joint of dual phase steel". Archives of Metallurgy and Materials, vol. 55, pp. 211-220, 2010.
- [8] E. Taban, A. Dhooge, E. Kaluc, "Plasma Arc Welding of Modified 12% Cr Stainless Steel", Materials and Manufacturing Processes, vol. 24, pp. 649-656, 2009.
- [9] M.St. Węglowski, S. Błacha, A. Philips, Electron beam welding – Techniques and trends – Review, Vacuum, vol. 130, pp. 72-92, 2016.
- [10] S.A.A.A Mousavi, A. Gharedaghi, et al., "Metallurgical investigations of laser welding of AISI 304 stainless steel". Materials Science Forum, vol. 580-582, pp. 41-44, 2008.
- [11] S.P. Rajan, S.S. Kumaran, "Friction welding of 304 austenitic stainless steel tube to tube plate joints using external tool". Journal of Advanced Mechanical Design, Systems, and Manufacturing, vol. 9, pp. 1-8, 2015.
- [12] R. Blondeau, Metallurgy and Mechanics of Welding Processes and Industrial Applications, ISTE Ltd and John Wiley & Sons, Inc., (2008). p. 419.
- [13] S. Saha, M. Mukherjee, T.K. Pal, "Microstructure, texture, and mechanical property analysis of Gas Metal Arc welded AISI 304 austenitic stainless steel". Journal of Materials Engineering and Performance, vol. 24, pp. 1125-1139, 2015.
- [14] Melting temperature ranges for stainless steels, www.bssa.org.uk/topics.php?article=103, accessed on 28.09.2016.